AGU ADVANCING EARTH AND SPACE SCIENCES

Geophysical Research Letters

RESEARCH LETTER
10.1029/2023GL103635

Key Points:

- The mean westward circumpolar motion of Jupiter's northern and southern polar cyclones is analyzed and explained by the β-drift effect
- Simulations show that the "center of mass" of a group of cyclones behaves like one equivalent cyclone, moving poleward-westward under β-drift
- This center-of-mass approach is applied to the Juno data, implying that the cyclones' collective β-drift drives their observed westward drift

Supporting Information:

Supporting Information may be found in the online version of this article.

Correspondence to:

N. Gavriel,
nimrod.gavriel@weizmann.ac.il

Citation:

Gavriel, N., & Kaspi, Y. (2023). The westward drift of Jupiter's polar cyclones explained by a center-of-mass approach. *Geophysical Research Letters*, *50*, e2023GL103635. https://doi.org/10.1029/2023GL103635

Received 10 MAR 2023
Accepted 29 AUG 2023

The Westward Drift of Jupiter's Polar Cyclones Explained by a Center-of-Mass Approach

Nimrod Gavriel[1] and Yohai Kaspi[1]

[1]Department of Earth and Planetary Sciences, Weizmann Institute of Science, Rehovot, Israel

Abstract The first orbits around Jupiter of the Juno spacecraft in 2016 revealed a symmetric structure of multiple cyclones that remained stable over the next 5 years. Trajectories of individual cyclones indicated a consistent westward circumpolar motion around both poles. In this paper, we propose an explanation for this tendency using the concept of beta-drift and a "center-of-mass" approach. We suggest that the motion of these cyclones as a group can be represented by an equivalent sole cyclone, which is continuously pushed by beta-drift poleward and westward, embodying the westward motion of the individual cyclones. We support our hypothesis with 2D model simulations and observational evidence, demonstrating this mechanism for the westward drift. This study joins consistently with previous studies that revealed how aspects of these cyclones result from vorticity-gradient forces, shedding light on the physical nature of Jupiter's polar cyclones.

Plain Language Summary The Juno spacecraft arrived at Jupiter in 2016, revealing a unique atmospheric phenomenon. Each of the poles of Jupiter is inhabited by a symmetrically structured group of cyclones, where a ring of cyclones surrounds one cyclone close to the pole. The collective observations of these cyclones over 5 years show that although they are relatively stable, they generally drift in the westward direction a few degrees per year. Here, we investigate the mechanism driving this drift by examining the cyclones as a group. This "center-of-mass" approach masks the interactions between the cyclones and only considers trends that happen simultaneously on all cyclones. Using model simulations, we show that the motion of a group's "center of mass" can be captured by a sole equivalent cyclone, pushed poleward and westward by the "beta-drift" effect, which is known to contribute to the motion of tropical cyclones on Earth. This westward force on the group as a whole is thus suggested as the driver of the observed westward drift. We conclude by presenting observational evidence supporting this hypothesis.

1. Introduction

The polar cyclones of Jupiter, revealed in 2017 by the Juno mission (Adriani et al., 2018; Bolton et al., 2017; Orton et al., 2017), are comprised of a single polar cyclone (PC) situated near each pole, and multiple circumpolar cyclones (CPCs), five at the south pole and eight at the north pole. The CPCs surround each PC in a ring at approximately latitude ±84° (Figure 1). While the cyclones were observed to retain a stable structure during the 5 years of measurements, slow motions about their mean positions, and a general westward trend were reported for both poles (Figure 1; Adriani et al., 2020; Mura et al., 2021, 2022; Tabataba-Vakili et al., 2020). The individual cyclones maintain maximum winds of up to ~100 m s^{-1} at ~1,000 km from their cores, and extend to diameters of about 5,000 km (Adriani et al., 2020; Grassi et al., 2018). While a stable configuration of CPCs was never observed before Juno's polar approaches, a PC has been persistently observed at each pole of Saturn (Baines et al., 2009). The formation of a PC on a gas giant is well understood and revolves around the concept of "beta-drift," which drives cyclonic vortices poleward (Adem, 1956; Fiorino & Elsberry, 1989; Rossby, 1948; Smith & Ulrich, 1990), where they converge and maintain a PC (Brueshaber et al., 2019; Hyder et al., 2022; O'Neill et al., 2015, 2016; Scott, 2011). This β-drift mechanism will be further explained in the following sections.

Given this polar attraction of cyclones, an additional mechanism is needed for explaining the existence of the stable Jovian CPCs, so that they would not merge at the poles. The gradient of planetary vorticity, β, is the driver of β-drift. It was shown that if, in addition to β, the vorticity gradient of the PCs is accounted for when considering β-drift, then the Jovian CPCs are located at a latitude (approximately ±84°) where the net vorticity gradient vanishes, and thus the CPCs are in a stable equilibrium (Gavriel & Kaspi, 2021). On Saturn, which is dynamically similar to Jupiter (Galanti et al., 2019; Kaspi et al., 2020; Showman et al., 2018), such equilibrium is currently unattainable, inhibiting stable CPCs (Gavriel & Kaspi, 2021). For the PCs to have a vorticity gradient with the

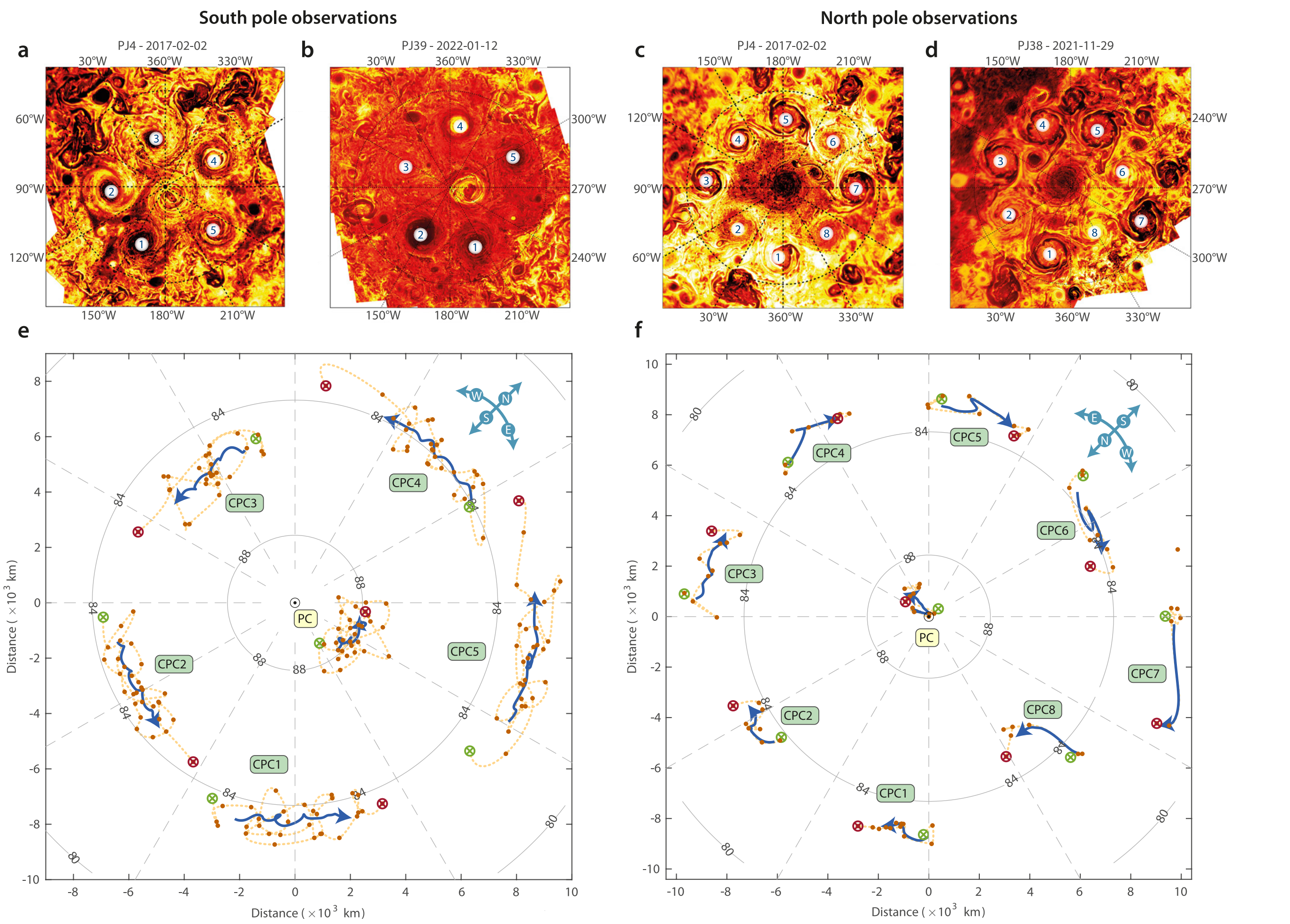

Figure 1. Observations of a westward drift in the north and south poles of Jupiter. (a–d) Infrared images of Jupiter's poles taken by the Jovian Infrared Auroral Mapper instrument onboard Juno. These panels were adapted from Mura et al. (2022). (a, b) Images from the south pole in February 2017 (panel a), and in January 2022 (panel b). (c, d) Images from the north pole in February 2017 (panel c), and in November 2021 (panel d). (e, f) Trajectories of the cyclones in the south (panel e) and north (panel f) poles, as observed over 5 years. The orange dots represent the observed locations during Juno's polar approaches (Mura et al., 2021, 2022). The dashed yellow curves represent an interpolation of the trajectories between observations. The green and red crosses represent the observed locations in February 2017 and 5 years later, respectively. The blue arrows represent a moving average of the interpolated trajectories, showing the overall westward trend experienced by the individual cyclones. The gray circles denote the 88°, 84°, and 80° latitude lines. The gray dashed lines represent increments of 30° longitude. The point (0, 0) represents the pole.

right direction to oppose β, they need to possess an anticyclonic "shielding" around them, as was shown using Shallow-Water (SW) simulations (Li et al., 2020).

1.1. Observed Motion of Jupiter's Polar Cyclones

In Figures 1e and 1f, the reported locations of Jupiter's polar cyclones (Mura et al., 2022) during the period 2017–2022 are presented. As direct observations of the north polar cyclones were much less frequent than those of the south, the trajectories of the north cyclones are much less constrained. Focusing on the better-determined trajectories at the south pole (Figure 1e), two trends become apparent. One motion trend is a mostly circular motion with a period of ~12 months and a radius of ~400 km (Gavriel & Kaspi, 2022). This motion was shown to follow a strong correlation between the instantaneous acceleration of each cyclone and the estimated total vorticity gradient under which it moves, suggesting that this motion is driven by the generalized β-drift mechanism (Gavriel & Kaspi, 2022). The second motion trend is an overall westward tendency of each cyclone (Blue arrows in Figures 1e and 1f), averaging to about 3° longitude per year at the north pole and 7° at the south (Mura et al., 2022). In this study, we provide an explanation for this westward trend by considering the generalized β-drift of all the polar cyclones at large. In the following section, we explain how one cyclone in a β-plane would feel an acceleration poleward and westward due to β-drift. Then, we suggest a "center-of-mass" (CM) approach where the aggregate motion of a group of cyclones can be estimated by the motion of one "equivalent cyclone" following the group's CM, which allows filtering the noisy interactions between the cyclones. Thus, the equivalent cyclone, orbiting the pole due to the poleward component of β-drift, would also precess westward due to the westward component of β-drift, projecting on the westward motion of the individual cyclones. We conclude our analysis with observational support for this hypothesis.

2. Poleward-Westward Acceleration of Barotropic Cyclones With a Background Vorticity Gradient

To understand how β-drift can cause the observed westward motion of Jupiter's polar cyclones, we start by reexamining the ideal case of a 2D (barotropic) cyclone under a linear change in background vorticity (β-plane). This scenario has been studied extensively in the past in the context of tropical cyclones on Earth, establishing the concept of β-drift, which is the generation of a dipole of vorticity (termed β-gyres) propelling cyclones in a tilted direction relative to the gradient of background vorticity (Adem, 1956; Fiorino & Elsberry, 1989; Rossby, 1948; Smith & Ulrich, 1990, 1993; Smith et al., 1990). Here, we illustrate the generation of the β-gyres by simulating, using the Dedalus solver (Burns et al., 2020), the secondary vorticity tendency according to the partitioning suggested by Smith et al. (1990). The scaled equation we solve is, at leading order,

$$\frac{\partial \xi_{\mathrm{g}}}{\partial t} = -\hat{\beta} v_{\mathrm{v}} - \mathbf{u}_{\mathrm{v}} \cdot \nabla \xi_{\mathrm{g}}, \tag{1}$$

where ξ_{g} is the secondary (generated) relative vorticity, and $\mathbf{u}_{\mathrm{v}}$ is a prescribed idealized vortex velocity vector with components $(u_{\mathrm{v}}, v_{\mathrm{v}})$ in the (x, y) directions, in a grid moving such that the vortex is always at the center (see Supporting Information S1 for the full equations and other model details; the used scale factors are supplied in Equation S6). The first term on the RHS, the advection of background potential vorticity by the vortex (originating from the curl of the Coriolis force), is proportional to the unit-less parameter $\hat{\beta} = \Delta f / \omega$, which is the ratio between the change in background vorticity across the core of the vortex ($\Delta f = \beta R$, where R is the radius of maximum velocity in the vortex), and the rotation frequency scale of the vortex ($\omega = V/R$, where V is the maximum velocity in the vortex). Thus, this parameter encapsulates how steep is the vorticity gradient across the cyclone, which in turn would determine the resulting magnitudes of ξ_{g}. In addition, the second term on the RHS of Equation 1 represents the subsequent advection of generated ξ_{g} by the primary circulation of the vortex. The full equation also contains the nonlinear terms, a numerical viscosity term, and a sponge term, which helps avoid effects from the double periodic boundaries.

In Figures 2a–2c, three simulation snapshots are plotted for ξ_{g}, resulting from the primary vortex circulation in a β-plane, as shown in Figure 2d. As the simulation begins from rest $\left(\xi_{\mathrm{g}} = 0\right)$, the only term generating vorticity immediately after $t = 0$ (Figure 2a) is the $-\hat{\beta} v_{\mathrm{v}}$ term, which changes according to the meridional velocity of the primary circulation. As such, near $t = 0$, we have a dipole oriented in the x direction, creating an initial acceleration northward (toward the gradient of background vorticity). This ξ_{g} generation is illustrated as the red and blue regions in Figure 2e, representing the advective flux of background vorticity by $\mathbf{u}_{\mathrm{v}}$. Then, this generated ξ_{g} dipole is twisted by $\mathbf{u}_{\mathrm{v}}$ (Figures 2b and 2c and orange and turquoise clouds in Figure 2e), accelerating the vortex in the westward direction. The direction of the β-drift velocity vector ($\mathbf{u}_{\beta}$) is determined by the diagonal line where the terms $-\hat{\beta} v_{\mathrm{v}}$ and $-\mathbf{u}_{\mathrm{v}} \cdot \nabla \xi_{\mathrm{g}}$ cancel each other. This direction is poleward-westward for cyclones with background vorticity increasing poleward, but would flip to equatorward-eastward if the background vorticity increases equatorward (Figure S1 in Supporting Information S1), such as in the case when the Jovian CPCs get too close to the shielded PCs (Gavriel & Kaspi, 2021, 2022).

An account of the acceleration of β-drift with time can be seen in Figure 2f, showing how the secondary velocities at the center of the cyclone (u_{β} and v_{β} in the x, y directions, respectively) are proportional to $\hat{\beta}$ for the majority of the acceleration phase. If the velocities were not scaled by $\hat{\beta}$, the different curves would have magnitudes proportional to $\hat{\beta}$, but this scaling fuses the curves together. The curves eventually separate due to the accumulation of non-linearities. This separation happens sooner for simulations with larger $\hat{\beta}$. The direction of $\mathbf{u}_{\beta}$ can be calculated from the two panels of Figure 2f as $\tan^{-1}(v_{\beta}/u_{\beta})$. The time is scaled by R/V, which is of order $\sim$3 hr for Jupiter's cyclones; the velocity is scaled by V, in addition to $\hat{\beta}$. It can be seen that the model is unstable for $\hat{\beta}$ values on the order of 5×10^{-2} and larger, which we assume to be due to the non-linear effects. The $\hat{\beta}$ values of

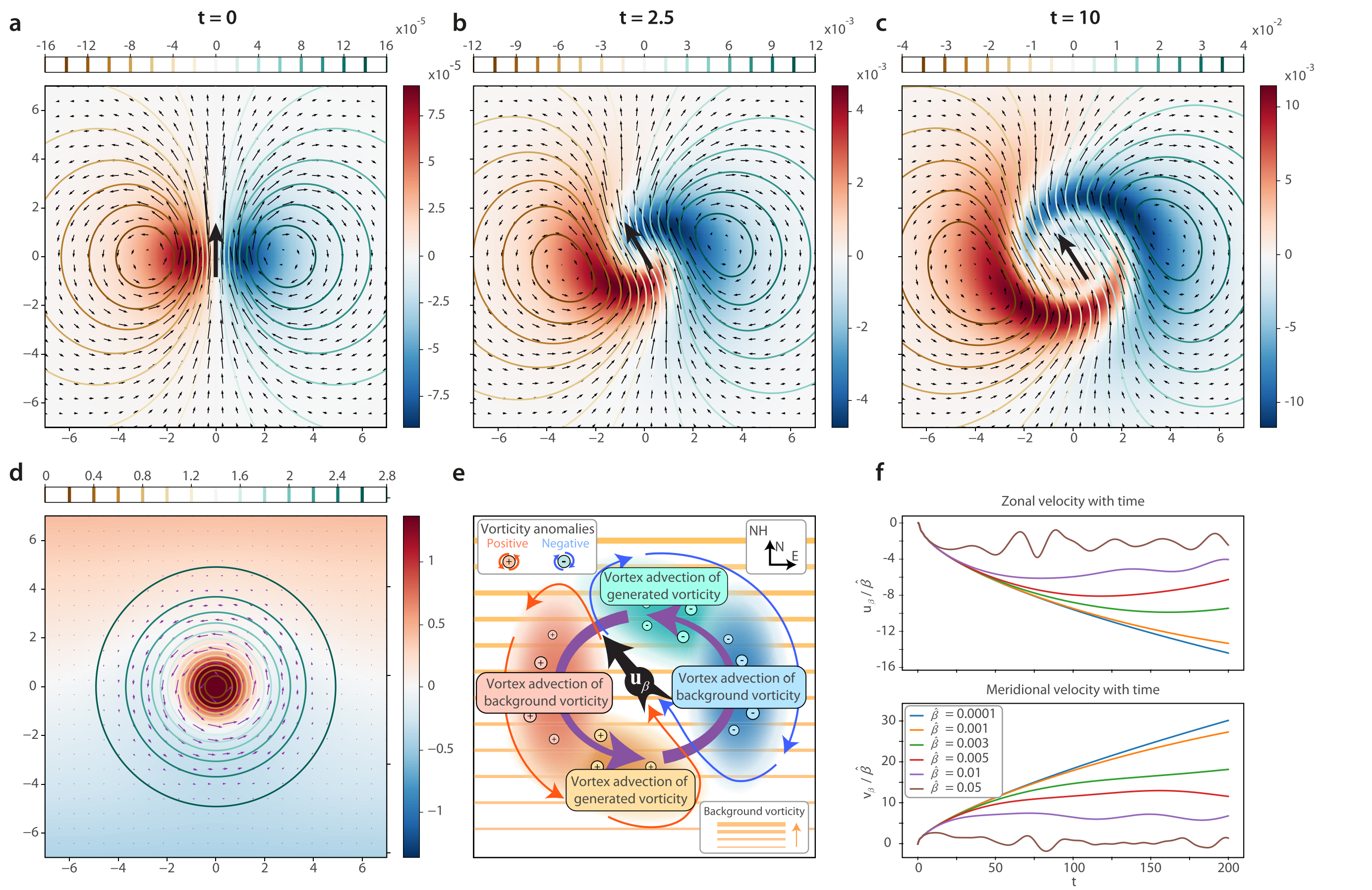

Figure 2. The mechanism for the westward component of β-drift. (a–c) Three snapshots from a simulation showing the development of a β-drift secondary circulation. The red-blue contours represent the generated vorticity. The brown-teal contours are streamlines. Black arrows represent the direction and relative magnitude of the generated velocity field, where the big central arrow represents the instantaneous β-drift advective velocity at which the cyclone is traveling. All the numbers are unitless, normalized by the respective cyclone characteristic parameters. (d) The same as panels (a)–(c), but for the primary cyclone circulation forcing the simulation. The north-south color gradient represents the gradient of background vorticity (for illustrative purposes, this gradient is enhanced relative to the values used in the simulation). A video of the simulation is available in Movie S1. (e) An illustration of the two main terms (×2 for each side) that determine β-drift, according to Equation 1. The purple arrow represents the cyclone's tangential velocity ($\mathbf{u}_v$). The orange lines represent the background vorticity, where thicker lines represent larger magnitudes. The red-orange (blue-turquoise) clouds with plus (minus) signs represent generation of positive (negative) vorticity. The red (blue) arrows represent the generated cyclonic (anti-cyclonic) secondary circulation. The black arrow is the resulting β-drift velocity. While this illustration is for the northern hemisphere, the same principles work for the southern hemisphere, where a poleward-westward drift is generated as well (see the equivalent Figure S1 in Supporting Information S1). (f) Time evolution of the simulated β-drift velocity at the center of the cyclone, divided by $\hat{\beta}$ (black arrow in the center of panels a–c). Different colors represent different $\hat{\beta}$ values, showing that for a significant period of the acceleration, the velocities are proportional to $\hat{\beta}$.

Jupiter's polar cyclones are between 10^{-4} to 10^{-3} (Figure 4), and thus are represented well by the linear solutions. Another thing to note here about the applicability of Figure 4f to the Jovian polar cyclones is that as the cyclones move around, the effective β under which they operate changes its magnitude and direction, resulting in a resetting (or partial resetting) of the β-drift phase seen in Figure 4f and limiting the late-time evolution of the β-drift.

3. The Center of Mass for a Group of Cyclones and the Motion of an Equivalent Cyclone

In previous numerical studies of tropical cyclones, it was shown that two identical cyclones on an f-plane may orbit each other due to their mutual interaction, but once a poleward background vorticity gradient (β) is introduced, both cyclones gain a poleward-westward motion, while their motion relative to one another stays the same as in the f-plane scenario (J. Chan & Law, 1995). Thus, it can be inferred that an equivalent cyclone positioned in the CM of the cyclones, moves according to β-drift while absorbing the mutual interactions. To test this idea further, we use Dedalus to solve the barotropic vorticity equation, this time without the partitioning to primary and secondary circulations as in Figure 2, so that

10.1029/2023GL103635

$$\frac{D\xi}{Dt} = -\beta v, \tag{2}$$

where $D/Dt = (\partial/\partial t + \mathbf{u} \cdot \nabla)$ is the material derivative, $\mathbf{u}$ is the velocity vector (with components u and v in the x and y directions, respectively) and $\xi = \nabla \times \mathbf{u}$ is relative vorticity. Similar to the model in the previous section, here also a numerical viscosity term and a trap term (analogous to the one used in Siegelman et al., 2022b) are added to the model.

Equation 2 is integrated on a β-plane from an initial condition of a group of 6 identical cyclones positioned according to the colored dots in Figure 3a (see full model specifications in Supporting Information S1). The dashed curves are the Cartesian trajectories of the six cyclones and the orange curve represents the motion of their CM, calculated as the arithmetic mean of the instantaneous positions of the cyclones. In addition, another simulation is presented where only one equivalent cyclone, identical to the cyclones in the group, begins its motion from the center of the group and follows almost the exact trajectory of the CM. Thus, the motion is decoupled into two contributions: one is the north-westward motion of each cyclone due to β-drift, taking only β into account, and the other is the mutual interactions between the cyclones, which are absorbed when following the CM. The slight difference between the trajectories of the CM and the equivalent cyclone likely owes to non-linearities. To evaluate how should the cyclones be weighted in order to determine the CM when cyclones are not identical, we derive a weight estimation (see derivation in Supporting Information S1) based on integrated vorticity gradient forces between two cyclones (Figure S2 in Supporting Information S1), leading to

$$W_i = \frac{e^{-\frac{L}{R_i}} R_i^{-4}}{\sum \left(e^{-\frac{L}{R_j}} R_j^{-4} \right)}, \tag{3}$$

where W is relative weight, i (or j) is the cyclone's index, L is an average distance between the cyclones and the sum is over all the cyclones in the group. With this weight estimation, two other test cases are performed (Figures 3d and 3e), similar to Figures 3a–3c, but where the cyclones vary in their sizes, leading to similar results.

The implication of this idealized case to Jupiter's polar cyclones is non-trivial due to, for example, variations in the cyclones' properties within the group and the non-linear background vorticity (which behaves like a cosine of latitude). Our hypothesis is thus (Figure 3f), that if we look at an equivalent cyclone in the polar case, this cyclone only feels the acceleration due to β-drift, with no dependence on the inter-cyclone interactions. This means that while a CPC would feel alternating poleward-westward and equatorward-eastward accelerations by β and by interactions with the vorticity gradient of the other cyclones (Gavriel & Kaspi, 2022), on average, the residual is only due to β. The poleward component of the β-drift on the CM's equivalent cyclone would then maintain an elliptical orbit around the pole, and the westward component would rotate this orbit in the zonal direction. It is therefore proposed that the projection back to the cyclones of this rotation is the mechanism behind the observed westward drift at Jupiter's poles. In the following section, we use Juno's observations to support this hypothesis.

4. The Center of Mass of the Polar Cyclones in the Observations

The most straightforward way to calculate the CM is by taking the arithmetic mean of the locations of all the polar cyclones (the Cartesian projected locations, (x, y); see Equation S1 in Supporting Information S1). To take into account the different sizes of the cyclones, which were previously estimated from Juno's observations (Adriani et al., 2020), we use Equation 3 for a weighted average of the Cartesian coordinates when determining the CM's trajectory along the period of the observations (See Supporting Information S1 for the calculation procedure and the used values). As the data from the north pole is too infrequent, we only use the data from the south pole for Figures 4a–4e (Mura et al. (2022); see Figure S3 in Supporting Information S1 for the equivalent north-pole figure, based on the existing observations). It can be seen (Figure 4a) that the CM's trajectory is indeed very clean, and possesses mostly the 12-month oscillations exhibited by the individual cyclones (Figures 4d and 4e, Gavriel and Kaspi 2022). This suggests that this 12-month mode of motion is mostly synchronized between the cyclones, and is therefore largely due to the motion of the CM (i.e., the first mode of motion where all cyclones oscillate together as a group). In both the zonal and meridional cases, short-period modes are suppressed for the CM (Figures 4d and 4e). When considering an elliptical orbit with a radial force in the direction of the pole

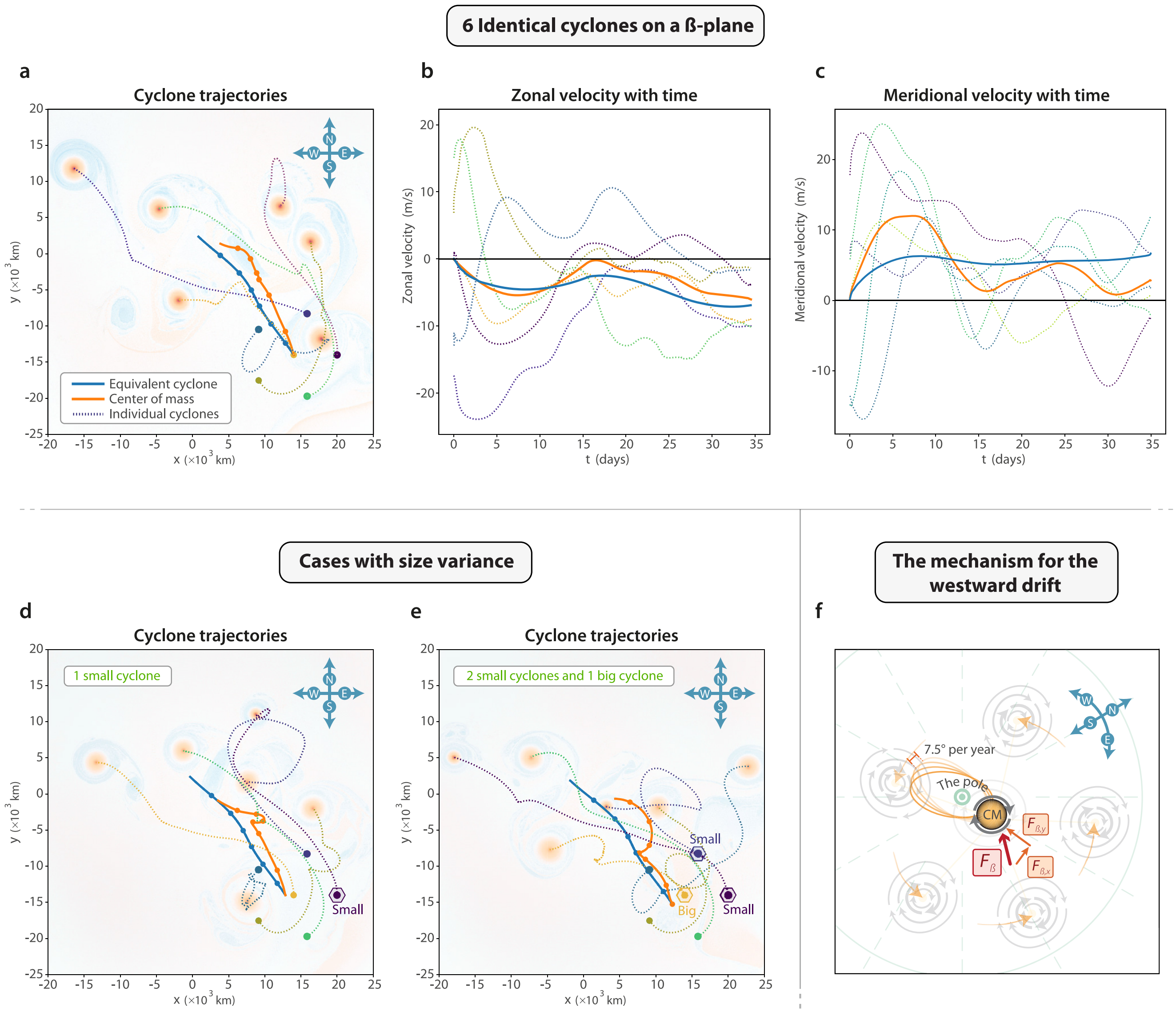

Figure 3. A center-of-mass (CM) approach for a group of cyclones. (a–e) The simulated motion of 6 cyclones on a β-plane and of their equivalent cyclone. (a) The Cartesian trajectories with time. The colored dots are the initial locations of six identical cyclones. The colored dotted lines are the trajectories of the individual cyclones. The orange (blue) curve represents the trajectory of the CM (equivalent cyclone), where the dots represent constant time intervals. The red-blue contours represent the relative vorticity map in the final snapshot. The colors are enhanced for illustrative purposes. (b, c) The same as panel a, but here, the abscissa is time and the ordinate is zonal and meridional velocity, respectively. (d) The same as panel a, but in this case one of the cyclones is smaller by 50%. (e) Another simulation, similar to panel a, where two cyclones are smaller by 50%, and one cyclone is larger by 20%. See Movie S2 for a video of the entire simulation of the six cyclones and Movie S3 for a video of the equivalent cyclone simulation (for the case with identical cyclones). (f) An illustration of how the poleward-westward β-drift acceleration can create a net westward drift in Jupiter's poles when looking from the perspective of a CM. The transparent cyclones represent the circumpolar cyclones. The red arrow is the β-drift acceleration, and the orange arrows are the meridional and zonal components. The orange ellipses illustrate the motion of the CM around the pole, where the ellipse precesses westward due to the zonal component of the β-drift.

(Figure 3f), the ellipse is expected to have its semi-major axis in the meridional direction. Consistently, the 12-month amplitude of the CM is larger in the meridional direction than in the zonal (Figures 4d and 4e).

One conflict between the hypothesis (Figure 3f) and the CM measurement (Figure 4a) is that the measured CM trajectory does not encompass the pole. This might be due to errors in estimating the weights of the cyclones (e.g., measurement errors, sparsity of data, and approximations in deriving Equation 3), which may also change in time during the observation period for the real cyclones. To test the sensitivity of the results (Figure 4) to the prescribed weights and the factor L (Equation 3), an analysis of randomly generated cyclone sizes is concluded, showing that the observation-based sizes significantly improve the results when comparing equivalent analyses

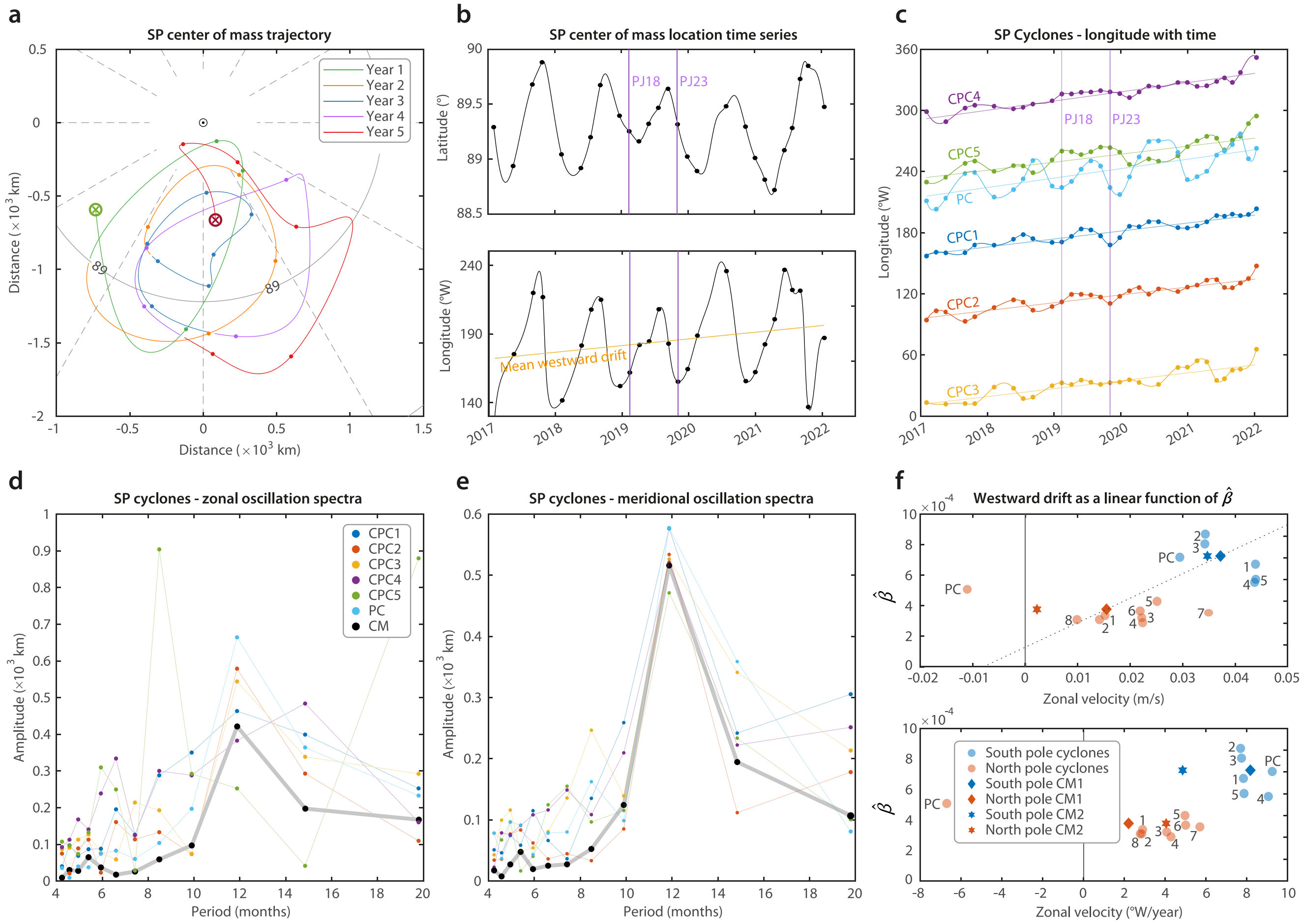

Figure 4. Calculations of the center-of-mass (CM) from the observations. (a) The Cartesian trajectory of the CM in the south pole of Jupiter according to the cyclone trajectories presented in Figure 1e (dots and curves represent real data and interpolation, respectively). The curve changes color with the passing of every year to illustrate the 1-year oscillatory motion exhibited in the CM's motion. (b) The latitude (upper panel) and longitude (lower panel) of the south CM with time. The purple vertical lines represent two incidents of an intruder cyclone during PJs 18 and 23. The orange line represents the linear fit of the westward location of the CM with time. (c) The longitude with time of each of the south polar cyclones. The straight lines represent linear fits for each cyclone, showing the westward motion. (d, e) The zonal and meridional oscillation spectra of the south polar cyclones (color) and of the CM (black). (f) The relation between the measured zonal velocities of the cyclones and $\hat{\beta}$. Zonal velocities are 5-year averages in metric units at the upper panel and longitude (°W) per year in the lower panel. Red and blue points represent values for the north and south poles, respectively. The numbers identify the respective circumpolar cyclones. The diamond and star shapes represent two different approaches for calculating the CM's zonal velocities, as discussed in the text.

with random or with identically sized cyclones (Figure S4 in Supporting Information S1). Also, investigating the role of the parameter L (Figure S5 in Supporting Information S1), we find that the used value of 6,000 km, representing an observationally based average distance between the cyclones (see Figures 1e and 1f), gives the best results in terms of how close is the CM's motion to encompassing the pole.

The time-series of the CM's motion (Figure 4b) indeed appears to have a clean sinusoidal form, where the inter-cyclone interactions of the individual cyclones (Figure 4c) are filtered. The linear fit for the CM's longitude with time (Figure 4b) has a slope of 8.17° longitude per year. The analogous linear fits for the individual cyclones (Figure 4c) have slopes of $8.23 \pm 0.71°$ longitude per year, suggesting that indeed the zonal drift of the cyclones is a projection of the CM's zonal drift (see the lower panel of Figure 4f for all values, including the north pole). Two reported incidents where an "intruder" vortex appeared in the south polar ring (PJ 18 and 23, Adriani et al., 2020; Mura et al., 2021) are marked (purple vertical lines in Figures 4b and 4c) as a possible explanation for the perturbations in the sinusoidal motion of the CM proximate to these observations.

Finally, the results from Figures 1–4 are tied together in Figure 4f. Here, the values of $\hat{\beta}$ for the cyclones and for the CM are estimated. As the effective β for the individual cyclones is close to zero, representing perturbations near stable equilibrium, the values of β (for estimating $\hat{\beta}_i$ of each cyclone i) are set equal for all of the cyclones and for the CM at each pole, and are determined by a vector sum of the β each cyclone is subject to (see Supporting Information S1). It can be seen (Figure 4f) that indeed $\hat{\beta}$ of the CMs in the north and south poles are proportional to their respective zonal motion. Here, we calculate the CM motion using two different methods (See Supporting Information S1 for the detailed calculations). For CM1, the velocities are the weighted (according to Equation 3) average of the individual cyclones' zonal velocities. For CM2, the velocities are calculated by a linear fit of the instantaneous zonal displacements of the CM. Using Figure 2f with the values of $\hat{\beta} \approx 7 \times 10^{-4}$, we get an overestimation in the scale of the zonal velocities of an order of magnitude relative to the south pole values in the upper panel of Figure 4f. Our interpretation of this discrepancy is that the steady state condition may have a form of dissipation that balances the β-drift acceleration at low values of zonal velocities, in addition to effects of the cyclones' depth, which can influence the results of Figure 2f (where the depth is set to infinity). Another consideration is a relative vorticity turbulent mixing that may reduce the vorticity gradient of one cyclone under another cyclone (Siegelman et al., 2022b) relative to our estimations, which are extrapolated from the profiles in the vicinity of the cyclones. Nevertheless, when using the method CM1 for the metric zonal velocity, which is the more physical form of velocity as related to the β-drift, it can be seen that both $\hat{\beta}$ and the CM's zonal velocity are approximately two times larger in the south pole than in the north pole (dashed line in the upper panel of Figure 4f). This proportionality is expected to be true regardless of dissipation or turbulent mixing, and provides support to the given hypothesis for the westward drift in Jupiter's poles.

5. Discussion

Since the discovery of Jupiter's polar cyclones, the role of vorticity gradient forces (or generalized β-drift), which takes into account both β and the relative vorticities of all neighboring cyclones, presented a consistent picture. These forces were used to explain the mean latitude of the cyclones and their number (Gavriel & Kaspi, 2021), the oscillatory motion patterns of the cyclones (Gavriel & Kaspi, 2022), and now their mean westward drifts as well. This series of studies, revealing different aspects of these forces, implies that these polar cyclones behave, to leading order, like discrete objects, linearly forced by a “spring-like” system driving them all in the poleward-westward direction while pushing them one from another. There are many uncertainties in the observations, such as variations between the velocity profile of each cyclone (and how it changes in time, Scarica et al., 2022) and the low resolution of the cyclones' tracks (Mura et al., 2022), especially in the north pole, in addition to complexities in the conversion of the CM concept from Cartesian to concentric polar coordinates and others.

However, we see that the CM of the cyclones has an organized motion (Figure 4), filtering the inter-cyclone exchanges as in the idealized case (Figures 3a–3e), and that the relative westward velocities of the CMs in the north and south poles, representatives of “equivalent” cyclones for the two groups, correlate with their different $\hat{\beta}$, as expected from the idealized cyclone simulations (Figure 2). These make the case that, indeed, the cumulative β-drift, integrated over all the cyclones in the group, is the mechanism for the observed westward drift of the cyclones. In this regard, we note that the westward drift in itself is surprising, since the PCs, if possessing considerable velocities as far equatorward as the CPCs, would advect the CPCs eastward around both poles. But, seeing that the longitudinal displacements are similar between the CPCs, the PCs and the CMs (lower panel of Figure 4f), we conclude that advective steering of the CPCs by the PC winds is unimportant, or is offset by the CM's westward drift. An important intuition for the contrast between the drift rates of the north and south poles can be derived from the fact that the ring of CPCs at the north pole is much more concentric (to the pole) than at the south pole (Figure 1). Therefore, the CM at the north is closer to the “rest” position at the pole, leading to a smaller β of the CM and a respectively smaller westward drift, than at the south. Thus, if the cyclones were put such that their CM rests exactly at the pole, no westward drift would be expected.

Another piece of important information that is still missing about these polar cyclones relates to the mechanism driving them and maintaining them against dissipation. In a recent barotropic numerical study, a step was taken in that direction, showing that initial small-scale turbulent conditions can “cool down” to form CPCs around a PC (Siegelman et al., 2022b). This study is in agreement with observational evidence showing that kinetic energy in the Jovian polar region follows an inverse energy cascade, where energy originating in small-scale turbulence is passed to the large-scale cyclones (Moriconi et al., 2020; Siegelman et al., 2022a). Regarding the depth of the cyclones, the β-drift framework, explaining many observations, suggests that the cyclones are deep (Gavriel & Kaspi, 2022). This is in agreement with the small Rossby number near the poles, suggesting the 2D Taylor-Proudman theorem regime (Busse, 1976; Vallis, 2017). However, there is still a gap toward understanding the mechanisms driving the cyclones, which might reveal what determines their size, strength and form. Finally, the unique conditions in Jupiter's poles, provided a striking opportunity to test, in the physical world, theories derived for explaining the motion of tropical cyclones on Earth (J. Chan & Law, 1995; Fiorino & Elsberry, 1989; Smith & Ulrich, 1990), where their transient nature and complex environment make the task of diagnosing their motion extremely difficult. These theories prove themselves consistently in Jupiter's polar cyclones, and assist in constructing the physical picture behind their surprising existence.

Data Availability Statement

No new data sets were generated during the current study. The data analyzed in this study were published by Mura et al. (2022) (DOI: https://doi.org/10.1029/2022JE007241), as cited in the text. The simulations were run with the Dedalus solver (Burns et al., 2020) (DOI: https://doi.org/10.1103/PhysRevResearch.2.023068).

Acknowledgments
This research has been supported by the Minerva Foundation with funding from the Federal German Ministry for Education and Research, the Israel Science Foundation (Grant 3731/21) and the Helen Kimmel Center for Planetary Science at the Weizmann Institute of Science. We thank Keren Duer, Eli Galanti, Or Hadas, Rei Chemke, and Quentin Nicolas for insightful conversations and helpful feedback.

References

Adem, J. (1956). A series solution for the barotropic vorticity equation and its application in the study of atmospheric vortices. *Tellus*, *8*(3), 364–372. https://doi.org/10.3402/tellusa.v8i3.9010

Adriani, A., Bracco, A., Grassi, D., Moriconi, M., Mura, A., Orton, G., et al. (2020). Two-year observations of the Jupiter polar regions by JIRAM on board Juno. *Journal of Geophysical Research: Planets*, *125*(6), e2019JE006098. https://doi.org/10.1029/2019je006098

Adriani, A., Mura, A., Orton, G., Hansen, C., Altieri, F., Moriconi, M., et al. (2018). Clusters of cyclones encircling Jupiter's poles. *Nature*, *555*(7695), 216–219. https://doi.org/10.1038/nature25491

Baines, K. H., Momary, T. W., Fletcher, L. N., Showman, A. P., Roos-Serote, M., Brown, R. H., et al. (2009). Saturn's north polar cyclone and hexagon at depth revealed by Cassini/VIMS. *Planetary and Space Science*, *57*(14–15), 1671–1681. https://doi.org/10.1016/j.pss.2009.06.026

Bolton, S. J., Adriani, A., Adumitroaie, V., Allison, M., Anderson, J., Atreya, S., et al. (2017). Jupiter's interior and deep atmosphere: The initial pole-to-pole passes with the Juno spacecraft. *Science*, *356*(6340), 821–825. https://doi.org/10.1126/science.aal2108

Brueshaber, S. R., Sayanagi, K. M., & Dowling, T. E. (2019). Dynamical regimes of giant planet polar vortices. *Icarus*, *323*, 46–61. https://doi.org/10.1016/j.icarus.2019.02.001

Burns, K. J., Vasil, G. M., Oishi, J. S., Lecoanet, D., & Brown, B. P. (2020). Dedalus: A flexible framework for numerical simulations with spectral methods. *Physical Review Research*, *2*(2), 023068. https://doi.org/10.1103/physrevresearch.2.023068

Busse, F. H. (1976). A simple model of convection in the Jovian atmosphere. *Icarus*, *29*(2), 255–260. https://doi.org/10.1016/0019-1035(76)90053-1

Chan, J., & Law, A. (1995). The interaction of binary vortices in a barotropic model. *Meteorology and Atmospheric Physics*, *56*(1), 135–155. https://doi.org/10.1007/bf01022526

Fiorino, M., & Elsberry, R. L. (1989). Some aspects of vortex structure related to tropical cyclone motion. *Journal of the Atmospheric Sciences*, *46*(7), 975–990. https://doi.org/10.1175/1520-0469(1989)046<0975:saovsr>2.0.co;2

Galanti, E., Kaspi, Y., Miguel, Y., Guillot, T., Durante, D., Racioppa, P., & Iess, L. (2019). Saturn's deep atmospheric flows revealed by the Cassini grand finale gravity measurements. *Geophysical Research Letters*, *46*(2), 616–624. https://doi.org/10.1029/2018gl078087

Gavriel, N., & Kaspi, Y. (2021). The number and location of Jupiter's circumpolar cyclones explained by vorticity dynamics. *Nature Geoscience*, *14*(8), 559–563. https://doi.org/10.1038/s41561-021-00781-6

Gavriel, N., & Kaspi, Y. (2022). The oscillatory motion of Jupiter's polar cyclones results from vorticity dynamics. *Geophysical Research Letters*, *49*(15), e2022GL098708. https://doi.org/10.1029/2022gl098708

Grassi, D., Adriani, A., Moriconi, M., Mura, A., Tabataba-Vakili, F., Ingersoll, A., et al. (2018). First estimate of wind fields in the Jupiter polar regions from JIRAM-Juno images. *Journal of Geophysical Research: Planets*, *123*(6), 1511–1524. https://doi.org/10.1029/2018je005555

Hyder, A., Lyra, W., Chanover, N., Morales-Juberías, R., & Jackiewicz, J. (2022). Exploring Jupiter's polar deformation lengths with high-resolution shallow water modeling. *The Planetary Science Journal*, *3*(7), 166. https://doi.org/10.3847/psj/ac7952

Kaspi, Y., Galanti, E., Showman, A. P., Stevenson, D. J., Guillot, T., Iess, L., & Bolton, S. J. (2020). Comparison of the deep atmospheric dynamics of Jupiter and Saturn in light of the Juno and Cassini gravity measurements. *Space Science Reviews*, *216*(5), 1–27. https://doi.org/10.1007/s11214-020-00705-7

Li, C., Ingersoll, A. P., Klipfel, A. P., & Brettle, H. (2020). Modeling the stability of polygonal patterns of vortices at the poles of Jupiter as revealed by the Juno spacecraft. *Proceedings of the National Academy of Sciences of the United States of America*, *117*(39), 24082–24087. https://doi.org/10.1073/pnas.2008440117

Moriconi, M., Migliorini, A., Altieri, F., Adriani, A., Mura, A., Orton, G., et al. (2020). Turbulence power spectra in regions surrounding Jupiter's south polar cyclones from Juno/JIRAM. *Journal of Geophysical Research: Planets*, *125*(7), e2019JE006096. https://doi.org/10.1029/2019je006096

Mura, A., Adriani, A., Bracco, A., Moriconi, M., Grassi, D., Plainaki, C., et al. (2021). Oscillations and stability of the Jupiter polar cyclones. *Geophysical Research Letters*, *48*(14), e2021GL094235. https://doi.org/10.1029/2021gl094235

Mura, A., Scarica, P., Grassi, D., Adriani, A., Bracco, A., Piccioni, G., et al. (2022). Five years of observations of the circumpolar cyclones of Jupiter. *Journal of Geophysical Research: Planets*, *127*(9), e2022JE007241. https://doi.org/10.1029/2022je007241

O'Neill, M. E., Emanuel, K. A., & Flierl, G. R. (2015). Polar vortex formation in giant-planet atmospheres due to moist convection. *Nature Geoscience*, *8*(7), 523–526. https://doi.org/10.1038/ngeo2459

O'Neill, M. E., Emanuel, K. A., & Flierl, G. R. (2016). Weak jets and strong cyclones: Shallow-water modeling of giant planet polar caps. *Journal of the Atmospheric Sciences*, *73*(4), 1841–1855. https://doi.org/10.1175/jas-d-15-0314.1

Orton, G. S., Hansen, C., Caplinger, M., Ravine, M., Atreya, S., Ingersoll, A. P., et al. (2017). The first close-up images of Jupiter's polar regions: Results from the Juno mission JunoCam instrument. *Geophysical Research Letters*, *44*(10), 4599–4606. https://doi.org/10.1002/2016gl072443

Rossby, C. (1948). On displacements and intensity changes of atmospheric vortices. *Journal of Marine Research*, *7*(175), 71.

Scarica, P., Grassi, D., Mura, A., Adriani, A., Ingersoll, A., Li, C., et al. (2022). Stability of the Jupiter southern polar vortices inspected through vorticity using Juno/JIRAM data. *Journal of Geophysical Research: Planets*, *127*(8), e2021JE007159. https://doi.org/10.1029/2021je007159

10.1029/2023GL103635

Scott, R. (2011). Polar accumulation of cyclonic vorticity. *Geophysical & Astrophysical Fluid Dynamics*, *105*(4–5), 409–420. https://doi.org/10.1080/03091929.2010.509927
Showman, A. P., Ingersoll, A. P., Achterberg, R., & Kaspi, Y. (2018). The global atmospheric circulation of Saturn. *Saturn in the 21st Century*, *20*, 295.
Siegelman, L., Klein, P., Ingersoll, A. P., Ewald, S. P., Young, W. R., Bracco, A., et al. (2022a). Moist convection drives an upscale energy transfer at Jovian high latitudes. *Nature Physics*, *18*(3), 1–5. https://doi.org/10.1038/s41567-021-01458-y
Siegelman, L., Young, W. R., & Ingersoll, A. P. (2022b). Polar vortex crystals: Emergence and structure. *Proceedings of the National Academy of Sciences of the United States of America*, *119*(17), e2120486119. https://doi.org/10.1073/pnas.2120486119
Smith, R. K., & Ulrich, W. (1990). An analytical theory of tropical cyclone motion using a barotropic model. *Journal of the Atmospheric Sciences*, *47*(16), 1973–1986. https://doi.org/10.1175/1520-0469(1990)047<1973:aatotc>2.0.co;2
Smith, R. K., & Ulrich, W. (1993). Vortex motion in relation to the absolute vorticity gradient of the vortex environment. *Quarterly Journal of the Royal Meteorological Society*, *119*(509), 207–215. https://doi.org/10.1002/qj.49711950910
Smith, R. K., Ulrich, W., & Dietachmayer, G. (1990). A numerical study of tropical cyclone motion using a barotropic model. I: The role of vortex asymmetries. *Quarterly Journal of the Royal Meteorological Society*, *116*(492), 337–362. https://doi.org/10.1002/qj.49711649206
Tabataba-Vakili, F., Rogers, J., Eichstadt, G., Orton, G., Hansen, C., Momary, T., et al. (2020). Long-term tracking of circumpolar cyclones on Jupiter from polar observations with JunoCam. *Icarus*, *335*, 113405. https://doi.org/10.1016/j.icarus.2019.113405
Vallis, G. K. (2017). *Atmospheric and oceanic fluid dynamics*. Cambridge University Press.

References From the Supporting Information

Chan, J. C., & Williams, R. (1987). Analytical and numerical studies of the beta-effect in tropical cyclone motion. Part I: Zero mean flow. *Journal of the Atmospheric Sciences*, *44*(9), 1257–1265. https://doi.org/10.1175/1520-0469(1987)044<1257:aansot>2.0.co;2